
HAMAMATSU PRESENTS
ANALYTICAL TALKS
WATCH NOW

Received: 20 March 2020 | Revised: 30 September 2020 | Accepted: 3 October 2020

DOI: 10.1002/jrs.6016

RESEARCH ARTICLE

Journal of RAMAN SPECTROSCOPY WILEY

Remote sensing of chemical agents within nuclear facilities using Raman spectroscopy

Michael Foster[1] | Michael Wharton[2] | William Brooks[1] | Matthew Goundry[2] | Charles Warren[1] | Jonathan Storey[1]

[1]IS-Instruments Ltd, Tonbridge, TN9 1SP, UK

[2]Jacobs, Warrington, WA3 6GN, UK

Correspondence
Michael Foster, IS-Instruments Ltd, Pipers Business Centre, 220 Vale Road, Tonbridge, Kent, TN9 1SP.
Email: mfoster@is-instruments.com

Funding information
InnovateUK; Sellafield Ltd

Abstract

The identification and characterisation of radioactive material and other hazardous substances are essential requirements for the nuclear industry. Raman spectroscopy can be used to identify substances; however, given the challenging nature of the environment, instruments typically cannot be located within 1 m of the target substance. A new stand-off Raman instrument using a spatial heterodyne spectrometer mounted on a remotely operated vehicle (ROV) is presented, and its ability to identify a range of chemicals of interest to the industry is demonstrated within a representative environment. The instrument demonstrated an ability to routinely make Raman observations at 1 m from the target with all sensitive electronic elements situated remotely outside the target environment.

KEYWORDS

instrumentation, nuclear facilities, spatial heterodyne spectrometer, stand-off Raman

1 | INTRODUCTION

The identification and characterisation of radioactive material and other hazardous substances within operating and decommissioning nuclear facilities are essential requirements for the industry.[1–3] Hazardous material (acids, alkalis and organic solvents) may be derived from multiple sources and may be present in several locations. They may have been stored in containers, tanks or silos, which have been in operation for several decades, and the composition of the remaining waste and the condition of the storage vessels are often unclear or unknown. Decommissioning these facilities involves processing waste into a form suitable for long-term storage (often by transferring it to a separate facility) and the monitoring of the processed waste to ensure there is minimal degradation of the processed material. In addition, many hazardous materials are used throughout the nuclear fuel processing cycle. Therefore, before the decommissioning of redundant facilities can commence, it is essential that all the hazardous material has been identified and removed.[3] Uncertainty regarding the presence and nature of this material presents significant safety concerns, which can lead to costly additional work or delays during postoperational clean out (POCO) operations.

Currently, hazardous substances are typically identified by the visual inspection of an experienced operator, who must then collect samples to be analysed. This is an expensive and potentially hazardous process. Therefore, in-situ identification of unknown samples that may be hazardous or indicative of corrosion without the need for direct human interaction is a clear advantage.

Any remote sensing method must be able to operate in a potentially harsh environment, coping with temperature, humidity and radiation issues that may be present. This demands that any environmentally sensitive systems must either be in protected housings or be located at a significant distance from the inspection target. The sensing equipment must be safe to operate in the environment, reliable, accurate and robust while also being user friendly, adaptable and flexible enough to be deployed in a wide range of complex facilities. Many of these facilities are very areas and have significantly restricted access and a complex architecture of pipework with vessels around which the probe must be manoeuvred in order to access the analysis points. It was determined that a 1-m measurement distance offered the best compromise between the need of probe head manoeuvrability, while maintaining a good level of signal to noise for the Raman system. With suitable equipment and experience, robotic deployment is a feasible mechanism for the implementation of chemical sensing technologies.

Raman spectroscopy has long been identified as a potential technique for remotely examining substances within nuclear facilities[3] including chemical spills and leaks. However, for any laser-induced spectroscopy system to be employed, several challenges must be overcome if the system is to be successfully deployed within the nuclear sector:

The system must be capable of Raman measurement at a distance of at least 1 m from the target due to potential access or environmental restrictions. The system must be compact, lightweight and portable such that it can be mounted on a remotely operated vehicle (ROV) for use in a variety of challenging deployment scenarios. There must be no risk of the laser igniting any substance within a facility. This requires the power density at the target to be strictly controlled. The system must also be able to make observations in timescales of less than 1 min on target samples that have an estimated thickness of ~200 μm (deposited smear).

This paper describes a new class of stand-off Raman spectrometer deployed on an ROV, which has been developed for this application. The Raman instrument could also be deployed via a robotic arm if required. The Raman probe section of the instrument was mounted on an ROV and combined with a 3-D vision stereo camera system[4] to view potential target samples. The 3-D vision system also provided ranging information to optimise the working distance of the probe and hence quality of the Raman signal captured.

The instrument has initially been tested against a series of materials of importance to the nuclear industry: Versamag, a Magnox sludge simulant, uranyl nitrate, tri-butyl phosphate (TBP) and kerosene, which are all present during reprocessing operations.[5–7] To the knowledge of the authors, this is the first time that stand-off Raman measurement have been made with a nuclear test facility, resolving all the unique challenges that this imposes.

2 | INSTRUMENTATION

The complete Raman system comprises three independent assemblies:

1. Raman spectrometer
2. ROV-mounted Raman probe
3. Raman excitation laser

The modular configuration of the Raman system allows for the electronically sensitive components to be situated externally from the target deployment environment. In practice, this results in the spectrometer and laser being placed externally and the Raman probe head being fixed to the ROV via a manipulatable interface and connected to both the spectrometer and laser via 15-m fibre optic cables (although longer cables may be used). This configuration allows for substantial spatial separation between the probe head and the other components of the system.

2.1 | The Raman spectrometer

Due to the inherent weakness of the Raman scattering process, molecules typically have Raman scattering cross sections in the order of 1×10^{-31} cm^2 sr^{-1} at 785 nm. Consequently, the spectrometer required by this application must provide excellent levels of sensitivity and therefore was critical to the success of the instrument in this application.

The strength of the captured signal for a given instrument is inversely proportional to the square of the distance to the target. The amount of the light expected from the target species is given by the LIDAR Equation 1

$$S = \frac{L_p V(R) A O_e D_{QE} I(R) \Delta R \alpha N e^{-2\tau}}{\pi R^2} \quad (1)$$

where L_p is the laser power, $V(R)$ is the overlap integral of the outgoing laser and the telescope field of view, A is the collecting telescope area, D_{QE} is the detector efficiency, ΔR is the depth of the sample being examined, α is the Raman scattering cross sections of the target species, O_e is the instrument optical efficiency, and N is the number of scattering centres, $I(R)$ is the overlap integral

between the outgoing and incoming beams, taking into account the obscuration of the secondary mirror as a function of distance to the target. τ is the optical depth of the medium between the instrument and the target, and R is the distance to the target.

This shows that high sensitivities at large stand-off distances can be achieved by increasing the laser power telescope diameter product. For example, pulsed laser Raman instruments have achieved very large stand-off distances when measuring a variety of species[8–12] in excess of 1 km. However, in a nuclear facility, pulsed instruments cannot be used due to the large power densities at the target. When using continuous wave (CW) lasers, stand-off Raman observations[13,14] have been demonstrated for measurement of nitrates and explosives from tens of metres up to 250 m using large 200-mm diameter telescopes.[15] Additionally, in this instance, the requirement for a low power density at the target poses significant challenges. Either the total laser power must be reduced or the spot at the target must be increased resulting in the target having a large *etendue* (see Section 2.4).

For the spectrometer to collect the maximum possible light from the target assuming the source is a Lambertian in nature and make observations of the required resolution, the spectrometer *etendue* must match or exceed that of the target. Table 1 demonstrates the magnitude of the challenge by showing the *etendue* of a number measurement scenarios including for the case outlined in this paper.

Case A in Table 1 uses a pulsed laser and a state-of-the-art high-throughput dispersive Raman spectrometer, with a slit width of <100 μm coupled to an F1:1.8 collection lens resulting in the system having an collection *etendue* of 1.9×10^{-9} m^2 sr, closely matching the observational requirement described within.[8] The same class of spectrometer was used within Case B. Case C is common example of a laboratory-based setup in which lower throughput spectrometer instruments can be used without experiencing any loss of light, using an F1:3 spectrometer.

However, in this application (Case D), the target *etendue* assuming an F1:10 collection telescope is 76 times greater than that of the dispersive spectrometer. This light will therefore be lost at the spectrometer entrance. One solution to this problem is to use a fibre-bundle-based spectrometer as is typically used in transmissio and spatially offset Raman applications.[16–18] As tens of meters of fibre length are typically required in this sector, these fibre bundles become impractical and difficult to manufacture. An alternative option is to use an interferometric solution, which allows for much larger throughput to be achieved due to the Jacquinot advantage.[19] However, these solutions are expensive and have precisely controlled moving parts.

Therefore, to achieve the required performance specifications and collect all the light from the target, a static Fourier transform (FT) spectrometer known as a spatial heterodyne spectrometer (SHS)[20] was selected. The instrument is assembled in a Michelson interferometer configuration with the mirrors replaced by reflective diffraction gratings.[21] The two wave fronts from the gratings pass through the beam splitter and then interfere to form a fringe pattern in space that can be passed through an FT algorithm to extract the spectral information.

The key advantage of this spectrometer design is that for a given resolution, it provides a 100-fold increase in *etendue*[21,22] than can be achieved compared with a traditional dispersive system and, unlike a traditional FT spectrometer, has no moving parts. The resolving power, R, of the instrument is the number of lines illuminated at the grating surface[22] given by

$$R = 2G_L W \tag{2}$$

where G_L is the number of lines per mm on the grating and W is the width of image at the grating surface. The signal-to-noise ratio of a given spectral line is given by

$$SNR = \frac{S_P}{\sqrt{\sum S_p + S + B + S_D}} \tag{3}$$

TABLE 1 *Etendue* computation for a number of Raman use cases

Case	Description	Distance to target	Diameter of spot at the target	*Etendue* (m^2 sr)	Telescope
A	Long range pulsed laser	1,752 m	300 mm	2.1×10^{-9}	300 mm diameter
B	Long range CW laser	250 m	64 mm	2×10^{-9}	200 mm diameter
C	Common micro objective Raman	50 mm	100 μm	8.65×10^{-10}	16.6 mm diameter (F1:3 system)
D	Nuclear sector requirement	1	5 mm	1.96×10^{-7}	100 mm diameter (F1:10 system)

Abbreviation: CW, continuous wave.

where S_p is the light from the target source, S is the total signal light from the source, which is not associated with the signal line, B is the background or contaminant light and S_D is the dark noise.

The spectrometer was coupled to the Raman probe with a 1-mm diameter fibre optic, 0.39 NA (with no slit being present within the spectrometer) giving an *etendue* of 3.7×10^{-7} m^2 sr, significantly larger than the requirement given in Table 1. An Andor iVac 316 charge-coupled device (CCD) was used as the detector, thus ensuring good levels of sensitivity were achieved. A Semrock long-pass filter was mounted both in the spectrometer and within the Raman probe head to eliminate extraneous laser light. A summary of the Raman instrument specifications is given within Table 2.

2.2 | The stand-off Raman probe

The application requires that the Raman probe head must be compact and lightweight to allow integration with the ROV or other suitable deployment platform. The probe was designed to collect and couple light into a 1-mm optical fibre. A schematic of the probe is given in Figure 1. This shows the that laser signal is passed through a Semrock clean-up filter and then transmitted via a forward-mounted mirror effectively forming an obscuration-configurated telescope arrangement. This positioning ahead of the main imaging lens reduces any unwanted Raman scattered light from the large fused silica collection lens, which can become a noise source with the SHS due to the multiplex disadvantage.[23] The probe head was developed with deployment into potentially radioactive environments in mind and therefore was designed to have smooth surfaces and an optical window to enable cleaning and potential enclosure within a disposable covering.

The stand-off probe could be manually set to stand-off distances between 0.5 and 1.5 m and was set to a fixed working distance of 1 m for all measurements presented. The probe was approximately 370 mm in length and 140 mm in diameter. An image of this probe is given in Figure 2.

TABLE 2 Raman spectrometer instrument specifications

Parameter	Value
Spectrometer	
Type	Spatial heterodyne spectrometer
Operating wavelength	785 nm
Gratings	150 g/mm
Spot size	15 mm
Resolution per pixel	2.83 cm^{-1}
Spectral range	400–2,800 cm^{-1}
Detector	Andor iVac CCD
Laser type	PD LD Boxx Raman laser
Laser power	500 mW (note 250 mW measured as output from optical fibre)
Fibre optic diameter	1 mm
Fibre optic NA	0.39
Fibre optic length	15 m
Raman probe	
Operating range	0.5–1.5 m manually variable (fixed at 1 m)
Mass	1.95 kg
Obscuration	<2%

Abbreviation: CCD, charge-coupled device.

2.3 | Raman excitation laser

For this application, the instrument operating wavelength was selected to be 785 nm to minimise fluorescent contamination while maintaining a good level of sensitivity. A 785-nm wavelength stabilised PD-LD Boxx Raman laser was selected as the source providing up to 500 mW of output power (note that the measured output was ~250 mW). To achieve the required power density, the laser was set to diverge resulting in a 5-mm spot at a distance of 1 m. This resulted in the target having a large *etendue* and hence the selection of the SHS to perform the Raman analysis.

2.4 | The remotely operated vehicle

The ROV used for these tests was the Wood ROV022 high-mobility platform. The ROV is a nuclear hardened tracked crawler with four independent drive pods that can be rotated allowing the system to climb over obstacles or alter its profile to fit within small spaces. Power and communication were delivered to the system via a trailed umbilical connection. This also included both the Raman excitation laser source and Raman receiving fibre couplings.

Removable top plates provide a mounting point for a variety of different instruments varying from manipulator arms to laser scanning systems. For these tests, a heavy-duty pan and tilt mechanism to which the probe was attached was fitted to the rear mounting point. A pan

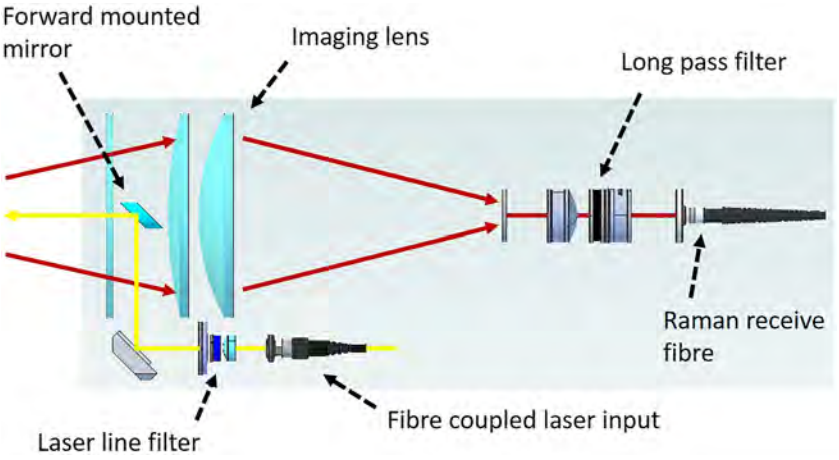

FIGURE 1 Schematic of the Raman probe [Colour figure can be viewed at wileyonlinelibrary.com]

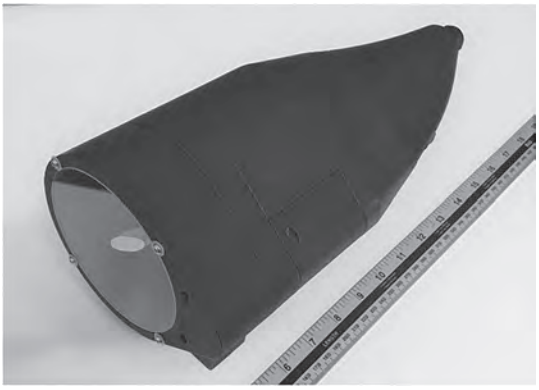

FIGURE 2 Raman probe with a fixed focus distance of 1 m

and tilt navigation camera mounted to the forward plate was used to both locate and confirm the pointing direction for the instrument. The Raman probe head was connected to the main spectrometer using a 15-m length 1-mm diameter optical fibre. A shielded fibre was used to transmit the Raman signal from the probe head to the spectrometer. This followed initial testing where it was observed that moderate levels of ambient light were leaking into the unshielded fibre. Figure 3 shows the ROV that was used for these trials in a variety of typical deployment scenarios. Ranging information was provided by a stereo camera unit provided by I3D Robotics mounted below the probe head.[24] This allowed the instrument to be accurately focused. However, it is important to note that this is just one of several potential deployment platforms and the overall system design deliberately included as much flexibility and modularity as possible. This is essential in order to provide the greatest possible scope for its use in the wide variety of scenarios found when characterising redundant nuclear facilities.

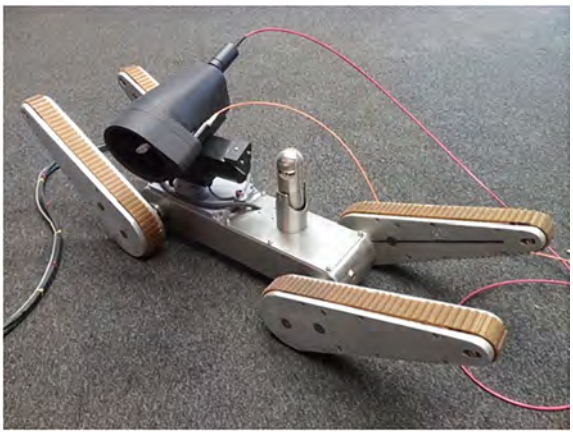

FIGURE 3 Fibre coupled Raman probe mounted on remotely operated vehicle (ROV) [Colour figure can be viewed at wileyonlinelibrary.com]

3 | RAMAN SPECTRA

To confirm the instrument sensitivity, Raman observations were made of cyclohexane, at a distance of 1 m. These were compared with previous studies of cyclohexane where estimates of its scattering cross section were obtained.[25,26] The spectrum was acquired within 0.1 s, consistently with expectations from Equation 1.

The system was then used to identify a number of chemicals of specific interest to the nuclear industry. This included a Magnox slurry simulant material (Versamag), uranyl nitrate, kerosene, TBP. To confirm the integrity of the data, the spectra of TBP and kerosene where compared with those given in the RRUFF database.[27] Mixed samples of TBP and kerosene were also examined to demonstrate the detection of multiple materials simultaneously. The liquid samples TBP and kerosene were measured as bulk samples, and the solids Versamag and uranyl nitrate were thin films (100–500 μm) on a substrate (glass, metal or plastic). All spectra have shown raw data with no data processing applied.

The ranging information provided by the stereo camera system guided the pan tilt mechanism to ensure that

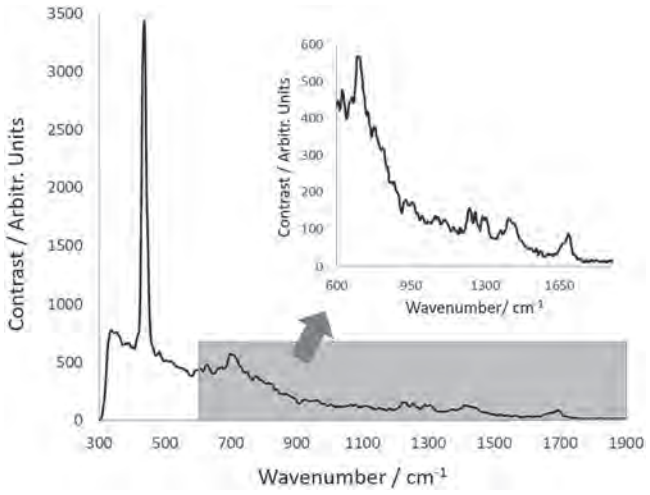

FIGURE 4 Raman spectra of Versamag from a range of 1-m observation was taken using an average of 3 frames with a 2-s integration time

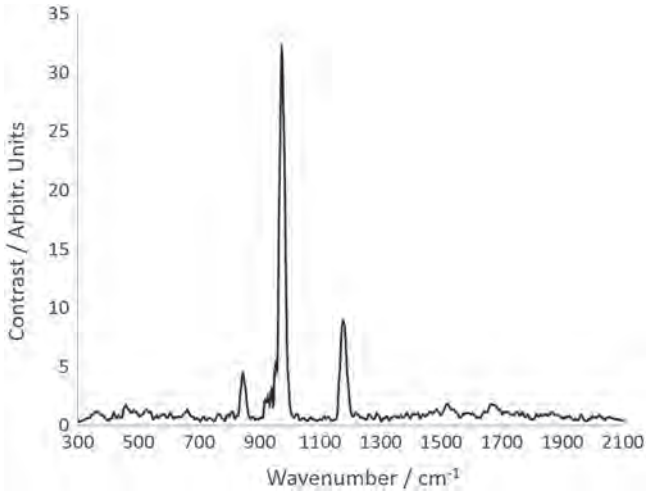

FIGURE 5 Raman spectra of uranyl nitrate from a range of 1-m observation was taken using an average of 3 frames with a 5-s integration time

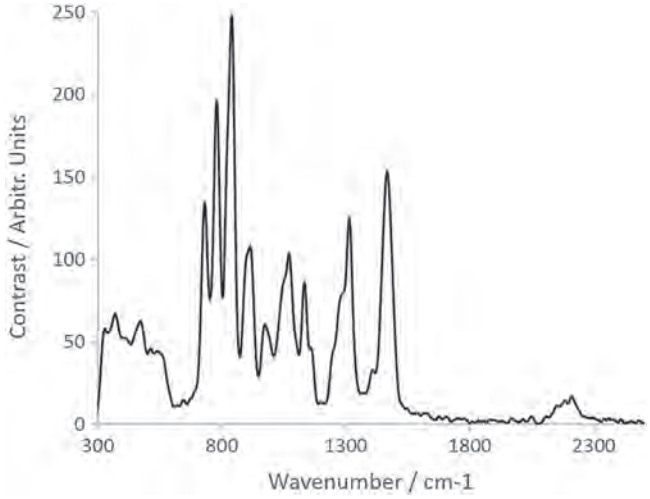

FIGURE 6 Raman spectra of 2 mm of tri-butyl phosphate from a range of 1-m observation was taken using an average of 3 frames with a 2-s integration time

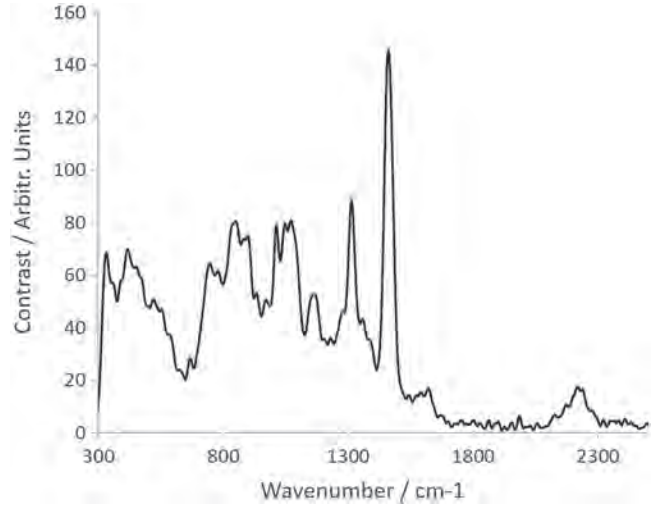

FIGURE 7 Raman spectra of a 2 mm of kerosene from a range of 1-m observation was taken using an average of 3 frames with a 2-s integration time

a 1-m stand-off range was maintained for all observations. The integration time was adjusted in each case to ensure that a good signal-to-noise regime was achieved.

Figures 4 and 5 show the Raman spectra of Versamag and uranyl nitrate, respectively. The Versamag sample was found to consistently present a prominent peak at approximately 475 cm^{-1}, in addition to several smaller peaks between 700 and 1,700 cm^{-1} as shown in the inset image in Figure 4. Also, clearly observable is a background response presenting as a baseline lift from low to high wavenumbers; this was suspected to be a fluorescence signal also from the sample found to overlay but not eclipse the Raman response.

The uranyl nitrate Raman spectrum shown in Figure 5 clearly indicates three prominent peaks at 845, 973 and 1,176 cm^{-1}, providing an excellent identifier for the material in a deployment scenario.

Figures 6 and 7 show the Raman spectra of TBP and kerosene. Good quality spectra were obtained for both samples.

As target samples in an operational environment are anticipated to contain both kerosene and TBP components, three mixed samples of varying ratios were also examined:

1. 10% vol TBP/90% vol kerosene
2. 20% vol TBP/80% vol kerosene
3. 50% vol TBP/50% vol kerosene

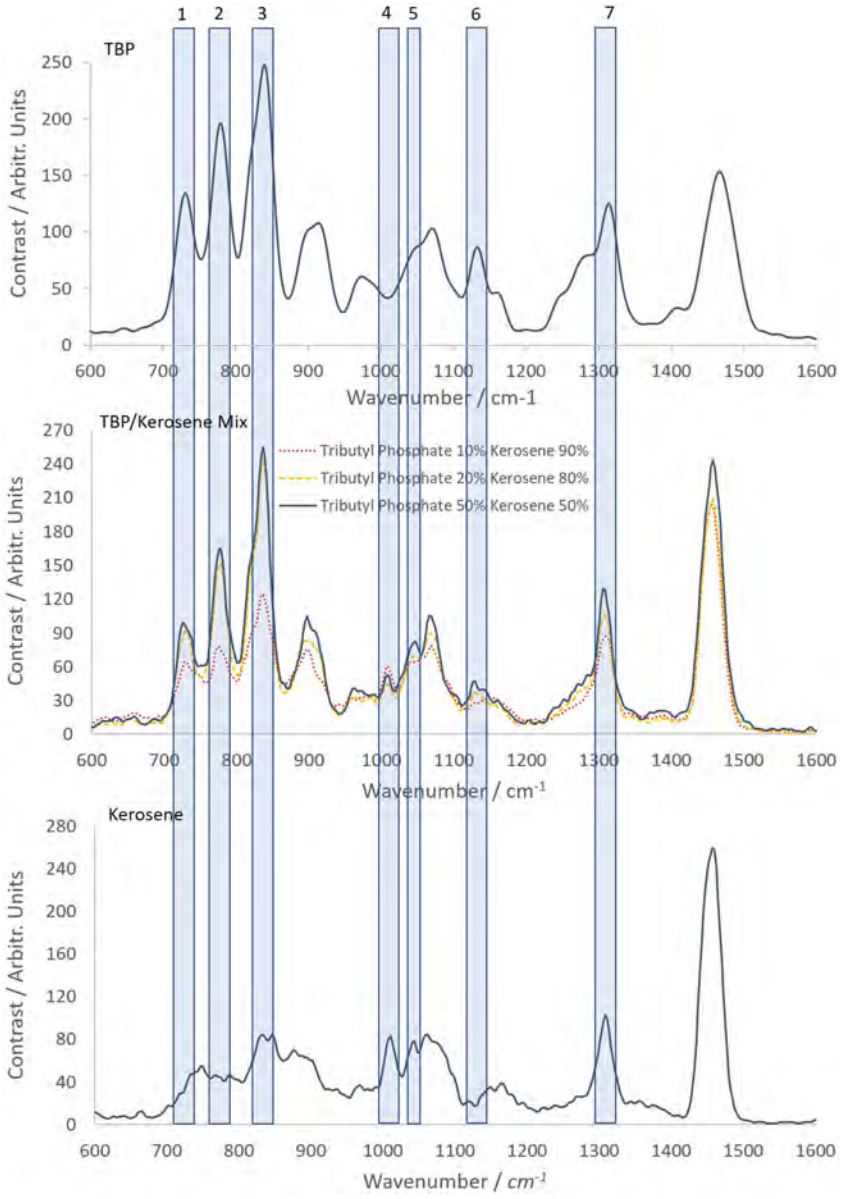

FIGURE 8 Top: Raman spectra of TPD. Middle: Raman spectra of three mixed samples: dashed red line = 10% tri-butyl phosphate (TBP) and 90% kerosene; dotted yellow line = 20% TBP and 80% kerosene; solid black line = 50% TBP and 50% kerosene. Bottom: Raman spectra of kerosene. Spectra acquired from a range of 1-m observation was taken using an average of 3 frames with a 2-s integration time [Colour figure can be viewed at wileyonlinelibrary.com]

Figure 8 shows a comparison of both TBP-only and kerosene-only samples in addition to the three mixed samples. To facilitate peak comparison and identify peaks that are unique to each material and peaks that appear common to both materials, a series of 10 highlighted bands has been overlayed. As labelled, Peaks 1–3 are unique to the TBP sample and are found to reduce in intensity as the TBP reduces in concentration in the sample. This is most observable in the 10% vol TBP/90% vol kerosene sample where the peaks most clearly reduce in intensity when compared with the two higher concentration samples. Peaks 1–3 also indicate that above 20% vol TBP, the intensity does not proportionally increase in intensity as a comparison between the 20% vol TBP/80% vol kerosene and 50% vol TBP/50% vol kerosene illustrates.

Peak 4 is unique to kerosene only and so could be readily used as an identifier for this material. Peak 5 appears predominantly unique to kerosene; however, some signal convolution is likely due to some Raman response also observed in the TBP sample at this Raman shift. Peak 6 is fully unique to the TBP sample and, with Peaks 1–3, can be used as a positive identifier of the presence of this material either in isolation or in a mixture as shown in the mixed sample spectra in Figure 8. Peak 7 is found in close proximity in both TBP and kerosene and also in the mixed samples where a convolution of Raman signals from both materials is observed. Therefore, this peak could be used to confirm the presence of TBP or kerosene but not specifically which of the two is present.

The mixed sample spectra presented in Figure 9 also indicates that the ratio of materials in the sample could

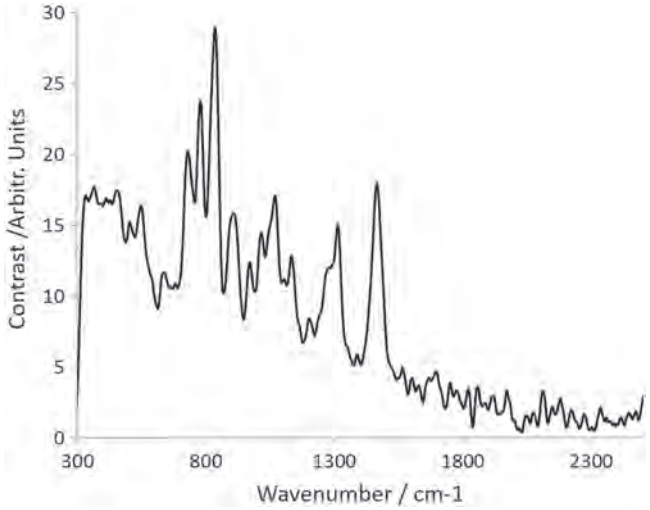

FIGURE 9 Smear of tri-butyl phosphate on stainless steel measured from a range of 1-m observation was taken using an average of 3 frames with a 10-s integration time

be approximated from the collected Raman spectra. In a real-case deployment scenario, it is anticipated that the observed Raman spectra could be analysed in real time using state-of-the-art convolutional neural network machine learning tools as described by Liu et al.[28]

Figure 9 shows the Raman spectra of a thin-film sample of TBP applied to a stainless steel surface (estimated to be 200 μm in thickness). This aimed to mimic a sample type typically found in a deployment environment and was therefore considered more representative than measuring bulk liquid samples as presented previously. The characteristic peaks isolated in Figure 9 are clear to observe. The baseline signal in this spectrum is found to be greater than in the data presented in Figure 6, due to the longer integration time required to observe the Raman signal, and so the increased contribution of background contaminant light. Furthermore, the baseline lift from lower to higher wavenumbers is likely a contribution from the substrate underlaying the target sample, highlighting the impact and importance of optimising the probe-to-sample working distance to maximise target sample Raman capture and minimise contaminant light from nontarget sources. It should also be noted that some fixed pattern noise can be observed beyond 1,700 cm^{-1} in the data; although this does not affect the results, this can be removed through accurate flat fielding and data processing techniques if required.[29]

4 | CONCLUSIONS

A novel, innovative stand-off Raman instrument mounted on an ROV has been demonstrated. The nuclear industry is expected to benefit from the development of this system, where numerous hazardous facilities with challenging access requirements for inspection equipment and personnel can be found across the world. The instrument has demonstrated the ability to identify target substances of interest to the nuclear industry at stand-off distances of 1 m. The instrument uses a 3-D stereo camera system to both locate possible targets and provide ranging information to guide the focusing position of the Raman probe to maximise the Raman signal.

The instrument is fibre coupled allowing elements that are sensitive to radiation or other potentially damaging environmental conditions to be mounted outside of the hazardous environment. This could allow the system to be deployed within a high-radiation waste facility with minimal nuclearisation while producing limited secondary waste. The system has been tested in a representative environment with observations made of a number of substances including uranyl nitrate, mixed organic liquids (TBP and kerosene) and a thin film of TBP on a stainless steel surface, aimed to mimic real-case examples in an operational environment.

ACKNOWLEDGEMENTS

The authors would like to thank InnovateUK and Sellafield Ltd for the funding and support on this project.

ORCID

Michael Foster https://orcid.org/0000-0001-7833-4500

REFERENCES

[1] https://www.gamechangers.technology/challenges/plant-characterisation/
[2] https://www.gov.uk/government/consultations/nda-radioactive-waste-management-strategy/outcome/radioactive-waste-strategy-september-2019
[3] H. G. M. Edwards, D. A. Long, I. T. Willis, *J. Raman. Spect.* **1995**, *26*, 757.
[4] J. Veitch-Michaelis, J. P. Muller, J. Storey, D. Walton, M. J. Foster, *Remote Sens. Spat. Inf. Sci.* **2015**, *XL4/W5*, 107.
[5] https://www.gamechangers.technology/challenges/post-operational-clean-out-poco/
[6] K. Nash, G. Lumetta (Eds), *Advanced Separation Techniques for Nuclear Fuel Reprocessing and Radioactive Waste Treatment*, 1st ed., Woodhead Publishing, Cambridge, UK **2011**.
[7] S. Farina, R. F. Schulz, G. Duffó, *International Workshop NUCPERF* 2012*: (RILEM Event TC 226-CNM and EFC Event 351)*, **2012**, Vol 56.
[8] A. K. Misra, T. E. Acosta-Maeda, J. N. Porter, M. J. Egan, M. W. Sanford, T. Oyamam, J. Zhou, *Appl. Spectrosc.* **2019**, *74*, 233.
[9] J. C. Carter, S. M. Angel, M. Lawrence-Snyder, J. Scaffidi, R. E. Whipple, J. G. Reynolds, *Appl. Spectrosc.* **2005**, *59*, 769.
[10] M. Gaft, L. Nagli, *Opt. Mater.* **2008**, *30*, 1739.

[11] S. K. Sharma, A. K. Misra, P. G. Lucey, S. M. Angel, C. P. Mckay, *Appl. Spectrosc.* **2006**, *60*, 871.
[12] N. Lamsal, S. K. Sharma, T. E. Acosta, S. M. Angel, *Appl. Spectrosc.* **2006**, *70*, 666.
[13] Y. Li, C. S. Cheung, S. Kogou, F. Liggins, H. Liang **2019;** 27. 31338
[14] S. M. Angel, T. J. Kulp, T. M. Vess, *Appl. Spectrosc.* **1992**, *46*, 1085.
[15] S. Sadate, C. Farley, A. Kassu, A. Sharma, *Am. J. Remote Sens.* **2015**, *3*, 1.
[16] P. Matousek, A. W. Parker, *Appl. Spectrosc.* **2006**, *60*, 1353.
[17] C. Eliasson, P. Matousek, *Anal. Chem.* **2007**, *79*, 8185.
[18] P. Matousek, A. W. Parker, *J. Raman Spectr* **2007**, *38*, 5563.
[19] R. J. Bell, *Introductory Fourier Transform Spectroscopy*, Academic Press, New York **1972**.
[20] J. Harlander, R. J. Reynolds, F. L. Roesler, *Astro. Phys. J.* **1992**, *396*, 730.
[21] M. J. Foster, J. Storey, P. Stockwell, D. Widdup, *Opt. Express* **2015**, *23*, 3027.
[22] M. J. Foster, J. Storey, M. A. Zentile, *Opt. Express* **2017**, *25*, 1598.
[23] J. M. Harlander, Thesis (Ph.D.) University of Wisconsin Madison, **1991**.
[24] J. Veitch-Michaelis, J. P. Muller, D. Walton, J. Storey, M. J. Foster, B. Crutchley, *International Archives of the Photogrammetry, Remote Sensing and Spatial Information Sciences,* **2016,** *XLI-B5*, 599
[25] M. O. Trulson, R. A. Mathies, *J. Chem. Phys.* **1986**, *84*, 2068.
[26] M. O. McAnally, B. T. Phelan, R. M. Young, M. R. Wasielewski, G. C. Schatz, R. P. Van Duyne, *Anal. Chem.* **2017**, *87*, 6931.
[27] https://rruff.info/
[28] J. Liu, M. Osadchy, L. Ashton, M. J. Foster, C. J. Solomon, S. Gibson, *Analyst* **2017**, *142*, 4067.
[29] C. R. Englert, J. M. Harlander, *Appl. Optics* **2006**, *45*(19), 4583.

How to cite this article: Foster M, Wharton M, Brooks W, Goundry M, Warren C, Storey J. Remote sensing of chemical agents within nuclear facilities using Raman spectroscopy. *J Raman Spectrosc*. 2020;51:2543–2551. https://doi.org/10.1002/jrs.6016